ELSEVIER

Tectonophysics 286 (1998) 253–271

TECTONOPHYSICS

Interpretation of crustal seismic velocities in the San Gabriel–Mojave region, southern California

Carey L. McCaffree Pellerin [a,*], Nikolas I. Christensen [b]

[a] *Department of Earth and Atmospheric Sciences, Purdue University, West Lafayette, IN 47907-1397, USA*
[b] *Department of Geology and Geophysics, University of Wisconsin, Madison, WI 53706, USA*

Received 6 February 1997; accepted 13 June 1997

Abstract

The increased concern over seismic hazards in the Los Angeles region has created interest in the crustal structure and mechanical properties associated with faults, like the Sierra Madre and San Andreas. This study presents the seismic properties of major lithologies found in the vicinity of the San Andreas fault zone in order to correlate with the Los Angeles Region Seismic Experiment (LARSE) results. Scientists from the LARSE group have recently acquired high-quality seismic data along three transects. Thirty-nine rock samples were collected along the LARSE Line 1, which trends NE–SW across the central Mojave Desert and the San Gabriel Mountains. These rock samples represent the following lithologies: Precambrian gneisses, San Gabriel anorthosite, Mesozoic granitic intrusives, Pelona schist, Mendenhall granulite gneisses and San Andreas fault zone cataclasites. The seismic properties were determined by measuring compressional and shear wave velocities as a function of confining pressure. Average compressional and shear wave velocities at 150 MPa show a wide range of values. The Mendenhall gneiss and the San Gabriel anorthosite complex have high velocities, 6.5 km/s and 6.4 km/s, respectively. The Pelona schist, the Mojave granitic intrusives, and the San Andreas cataclasitic rocks have average velocities of 5.8 km/s, 5.2 km/s, and 5.1 km/s, respectively. Average densities range from 2320 kg/m^3 for fault zone cataclasites to 3100 kg/m^3 for a Mendenhall granulite gneiss. Gneisses and schists show significant seismic anisotropy (5–20%) due to preferred mineral orientation, while most other rocks are nearly isotropic. Poisson's ratios range from a high of 0.29 in the San Gabriel anorthosite to a low of 0.22 in the San Gabriel gneiss. Comparison of the measured seismic properties with the LARSE velocity model allows interpretation of crustal structure in terms of rock compositions. The upper crust southwest of the San Andreas fault contains granitic intrusives, gneisses and schists, while under the Mojave Desert, the upper crust is dominated by gneisses. High velocities under the San Gabriel Mountains represent either lower crustal granulites or anorthosite. The velocity decrease beneath the San Andreas fault zone originates from minor amounts of cataclasite or the presence of low-velocity lithologies such as Pelona schist.

Keywords: seismic velocities; southern California; crustal structure; Poisson's ratios; San Andreas fault

* Corresponding author. Fax: +1 (317) 496-1210; E-mail: carey@crust.eas.purdue.edu

0040-1951/98/$19.00
PII S0040-1951(97)00269-2

1. Introduction

Recently, programs assessing earthquake hazards have focused on determining the physical properties and mechanical behavior associated with active fault zones and their surroundings (e.g., Page et al., 1992). Accomplishing this objective requires integrating geological and geophysical studies into a crustal model that characterizes fault properties. Such a model has been developed to characterize the central San Andreas fault. This model describes a low-velocity zone, which is 3 km wide, 10–15 km deep, filled with fault gouge, and deforming by continual creep Healy and Peake, 1975; Stewart and Peselnick, 1978; Feng and McEvilly, 1983; Wang, 1984; Shedlock et al., 1990; Eberhart-Phillips and Micheal, 1994). Geologists and geophysicists are currently developing a crustal model for southern California faults (Fig. 1); however, doing so is difficult due to the complex geology of the region (Ehlig, 1975; Dibblee, 1975; Roller and Healy, 1963; Hadley and Kanamori, 1977; Malin et al., 1981; Hearn and Clayton, 1986). The Los Angeles Regional Seismic Experiment (LARSE) collected high-quality seismic data along three transects, to better describe these complexities in geology. Of particular interest to this study is the LARSE high-resolution Line 1, which defines the compressional velocity structure across the San Gabriel Mountains and the Mojave Desert (Fuis et al., 1996). The LARSE results provide descriptions of the crustal structures and seismic velocities; however, the interpretation of seismic data in terms of rock composition requires rock seismic properties from laboratory studies.

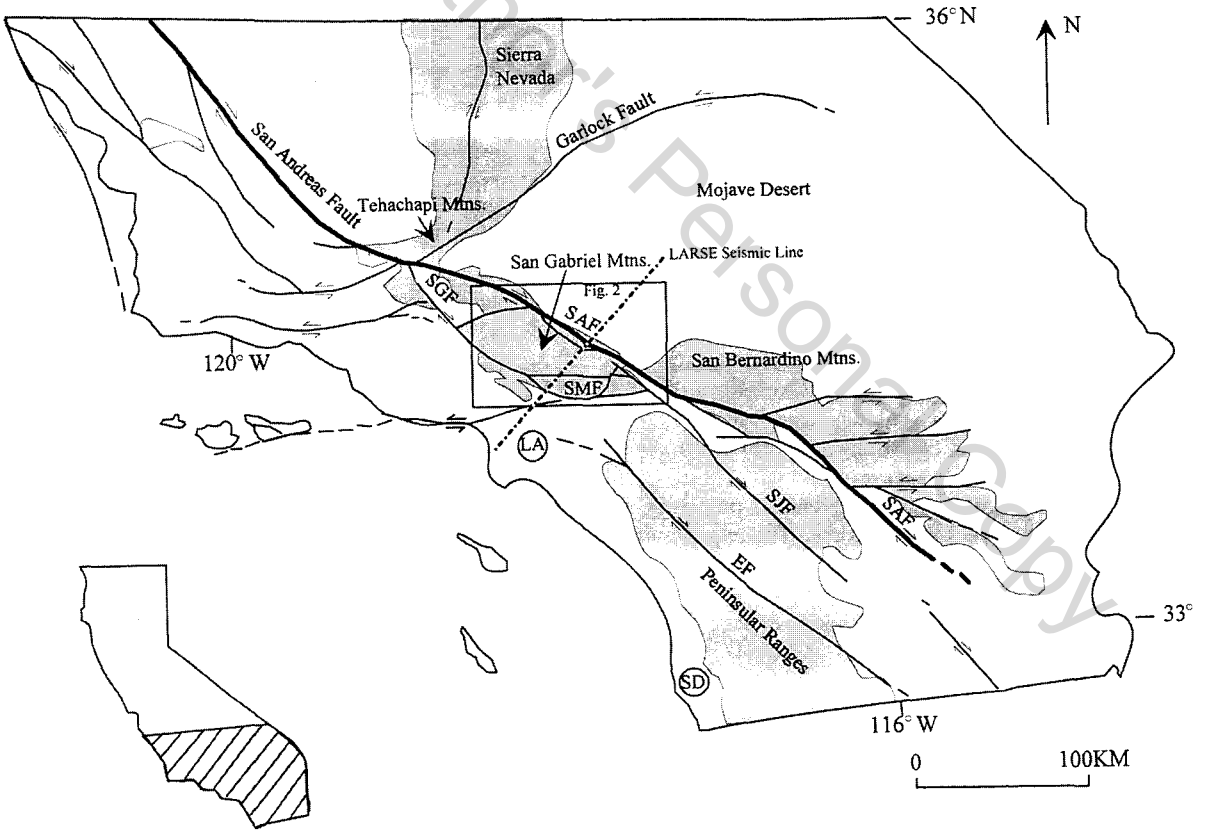

Fig. 1. Map of the Cenozoic fault segments in southern California (modified from May, 1989). Gray areas represent outcrops of crystalline rocks (not shown in the Mojave region). The dashed line marks the location of the LARSE line 1 seismic profile. The box represents the San Gabriel–Mojave region. *LA* = Los Angeles; *SD* = San Diego; *SGF* = San Gabriel fault; *SMF* = Sierra Madre fault; *SAF* = San Andreas fault; *SJF* = San Jacinto fault; *EF* = Elsinore fault.

This study discusses the seismic properties of major lithologies found in the San Gabriel–Mojave (SG-M) region, and interprets the LARSE seismic velocity model in terms of rock composition. The SG-M region (Fig. 1) includes the San Gabriel Mountains and the Mojave Desert, which are separated by the San Andreas fault. This region was selected because of its proximity to the LARSE seismic transect, accessibility to rock exposures, and propensity for future seismic activity. The seismic characterization was obtained through detailed laboratory analysis of rock samples, including petrographic descriptions and measurements of density, compressional and shear wave velocities, anisotropy, and Poisson's ratio. Results from this study will provide important constraints on the geology beneath the SG-M region, allowing for better assessment of earthquake hazards.

2. Geologic setting

The San Gabriel–Mojave (SG-M) region represents the center of the east–west-trending transverse ranges. Two basement terranes characterize the SG-M region, the San Gabriel terrane and the Mojave terrane (Ehlig, 1981). The Mojave terrane represents the original North American basement, whereas the San Gabriel terrane is an allochthon isolated by Cenozoic deformation along the San Gabriel and San Andreas faults. The rocks found in both terranes are similar: containing Precambrian gneisses that are intruded by Mesozoic granitic plutons, and followed by subsequent Cenozoic sediment deposition and deformation. The detailed geologic descriptions for each major lithology in the basement terranes are presented in Table 1. Fig. 2, after Woodburne (1975) and Ehlig (1981), shows the distribution of these lithologies across the SG-M region. The Cenozoic sediments will not be addressed because they are shallow features and have minimal influence on crustal structure.

The tectonic interpretation of the SG-M region is key for understanding the crustal structures related to convergent margins and transform faults. In the San Gabriel terrane, it is generally accepted that a Late Cretaceous magmatic arc was thrust over a shallow ocean basin putting crystalline basement on top of Pelona schist. The direction of thrusting and the eastward extent of the basin, however, is still poorly understood. Seismic reflection data suggest that the Rand schist, found along the Garlock fault, may correlate with the Pelona schist, implying eastward continuance of both the basin and the thrusting beneath the Mojave terrane (Cheadle et al., 1986; Li et al., 1992). However, recent drilling in the Mojave at Cajon Pass produced a geologic section containing gneisses and granitic intrusives with no evidence of Pelona schist (Silver and James, 1988). This suggests that the Mojave terrane, in contrast to the San Gabriel terrane, exhibits a simpler tectonic history as part of the stable North American craton. The Pelona schist is also used to reconstruct the Cenozoic deformation along the San Andreas fault. The 300 km of right-lateral displacement is inferred along the San Andreas fault during the Cenozoic by correlating of the Pelona schist with the Orocopia schist in the Chocolate Mountains (Ehlig, 1981).

The San Andreas fault is a dominant geologic feature in the SG-M region, cutting the region in half and juxtaposing the San Gabriel and Mojave terranes. In conjunction with 300 km of lateral displacement along the San Andreas, there is evidence for additional folding and faulting within the basement terranes. The lateral deformation of the San Andreas is accommodated by a braided system of thin faults (<50 m) isolating slivers of undeformed country rock (Woodburne, 1975; Dibblee, 1982). The rocks found in these thin faults are cataclasites, not fault gouge (Anderson et al., 1980). These thin cataclasitic faults may explain why stronger-magnitude earthquakes occur along this locked segment of the San Andreas.

3. Experimental techniques

3.1. Sample descriptions

Correlation of the rock seismic properties with the LARSE seismic data requires samples that accurately represent the geology along the LARSE profile. Fig. 2 shows the location of the 39 samples collected across the SG-M region for this study. These samples were selected to represent the major internal compositional variations of each lithology described in the region. For example, the San Gabriel gneiss samples are both felsic and mafic. Although sam-

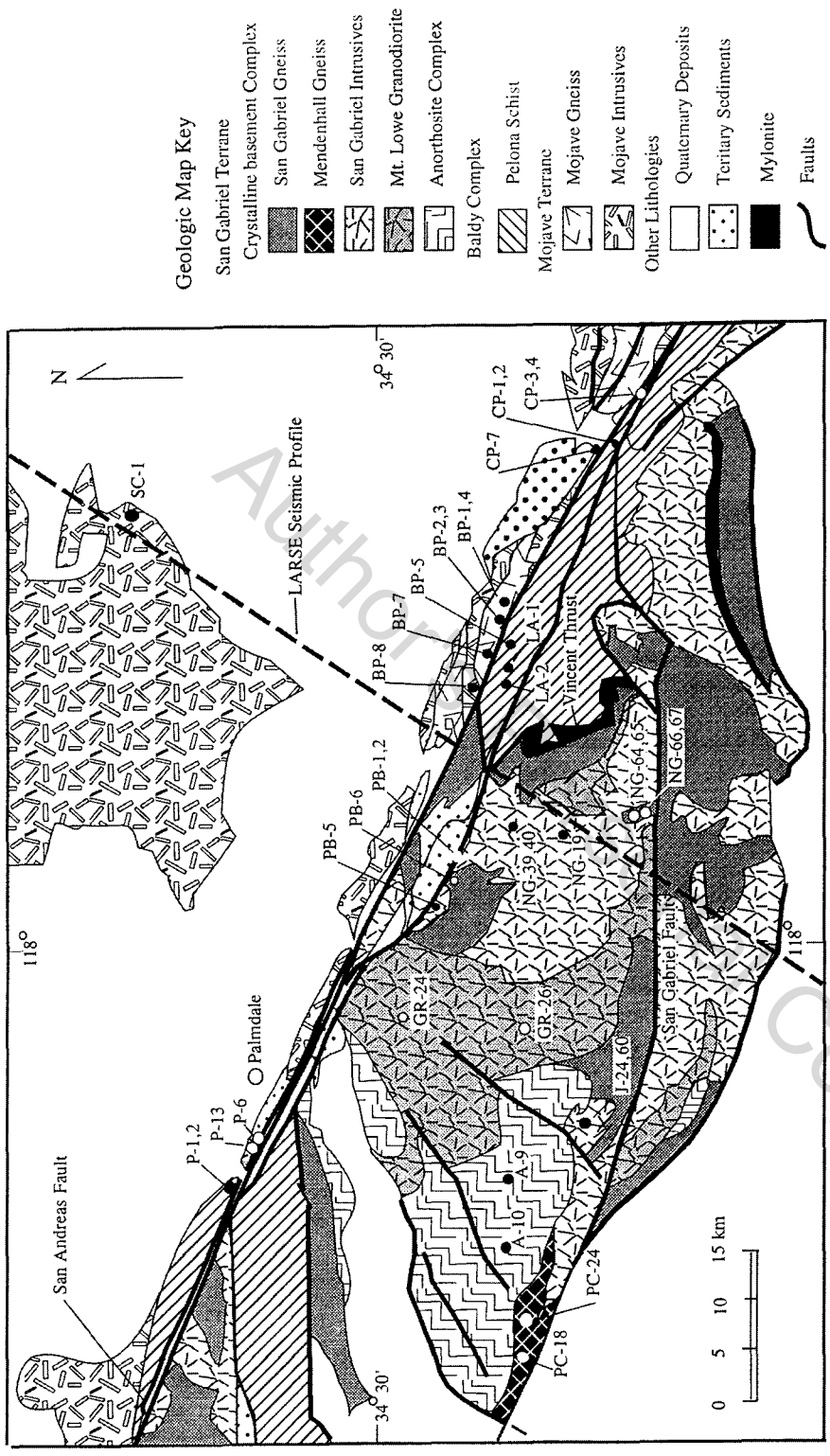

Fig. 2. Geologic map of the San Gabriel–Mojave region (modified from Woodburne, 1975). Marked on the map is the LARSE seismic profile of Line 1 as a dashed black line and sample locations as dots with corresponding sample numbers.

Table 1
Geologic summary of the major lithologies in the SG-M region

Lithology	Tectonic event	Description	References
San Gabriel terrane			
Paleoproterozoic:			
Gneisses	Regional metamorphism	Interfingered quartzo-feldspathic and amphibole-rich layers	Ehlig (1981)
Mesoproterozoic:			
San Gabriel anorthosite	Magmatic intrusion	Anorthosite with minor amounts of gabbro and syenite	Carter and Silver (1972)
Mendenhall gneiss	Thermal aureole produced during anorthosite intrusion	Granulite gneiss containing mafic and felsic components	Ehlig (1981)
Late Triassic:			
Mount Lowe intrusives	Magmatic intrusion	Granodiorite containing abundant feldspar with a zoned outer margin	Ehlig (1981); Barth and Ehlig (1988)
Cretaceous:			
Intrusives	Magmatic arc	A series of plutons varying in composition from granitic to dioritic	Barth (1990)
Late Cretaceous:			
	Regional compression caused thrusting along the Vincent fault and produces Pelona schist	Vincent fault is marked by a km-wide mylonite zone metamorphosed to greenschist grade	Crowell (1981); Jacobson (1988)
Pelona schist		Greenschist-grade quartz-mica schist with a layer of actinolite-epidote schist at the base of the thrust	Dibblee (1982); Jacobson (1988)
Mojave terrane			
Paleoproterozoic:			
Gneisses	Regional metamorphism	Interlayered quartzo-feldspathic and amphibole-rich gneisses with isolated layers of marble and mica schist	Burchfield and Davis (1981)
Cretaceous:			
Intrusives	Magmatic arc	A series of plutons varying in composition from granitic to dioritic	Burchfield and Davis (1981)
San Andreas fault zone			
Cenozoic:			
Cataclasites	Lateral displacement along the San Andreas fault	A braided system of thin cataclasitic faults isolating silvers of undeformed country rock	Anderson et al. (1980); Dibblee (1982)

pling the San Andreas fault rock was difficult due to intense weathering, a few cataclasites were obtained. Table 2 shows the coverage of samples relative to the internal compositional variations and the estimated surface distribution of these compositional variations by percent volume within each lithologic unit. The estimated surface distribution of each lithology is within 10% (A. Barth, pers. commun.). The percent surface volume distributions are used as weighting factors during the averaging of measured properties.

The mineralogy of each sample was estimated by visual analysis of a single petrographic thin section made from a core end (Table 3). The intrusive rocks were classified using the IUGS (1973) plutonic rock

Table 2
Lithologic distribution

Range of compositions	Estimated volume % at surface	No. of samples samples
Southwest of San Andreas (San Gabriel)		
Gneiss:		
Quartzo-feldspathic	50	4
Mafic	50	3
Mendenhall gneiss:		
Quartzo-feldspathic	50	1
Mafic	50	1
Intrusives:		
Granite	45	4
Diorite	45	1
Granodiorite	10	1
Mt. Lowe intrusive:		
Granodiorite	100	2
Anorthosite complex:		
Anorthosite	62	1
Gabbro	8	1
Syenite	30	1
Pelona schist:		
Quartz-mica	90	4
Actinolite-epidote	10	3
Northeast of San Andreas (Mojave)		
Gneiss:		
Quartzo-feldspathic	48	2
Mafic	48	1
Marble	4	2
Intrusives:		
Granite	25	2
Granodiorite	50	1
Diorite	25	1
San Andreas fault zone:		
Cataclasites	100	3

classification. Foliations or deformational features are observed in the gneisses, schists, and cataclasites, while all other samples exhibit randomly distributed equant grains. Gneisses and schists show strong foliations defined by preferred orientation of micas and amphiboles. The cataclasites exhibit intense deformation through fracturing and alteration.

3.2. Methods

The physical properties measured on the SG-M samples at the Purdue University Rock Physics Laboratory include: density, seismic anisotropy, and compressional and shear wave velocities. To determine seismic velocities and anisotropy, three perpendicular minicores (A, B, C), 2.5 cm in diameter and 4–6 cm in length, were cored from each sample. For metamorphic samples the axes of the A-cores are oriented normal to foliations. The B- and C-cores are cut parallel to the foliations and perpendicular to one another. The axes of B-cores are parallel to the strike of lineations, when present. Bulk densities are calculated from core dimensions and weights. Velocity measurement preparation includes jacketing the cores in copper, attaching brass tabs on the core ends, and inserting this assembly in rubber tubing to prevent oil saturation during the high-pressure runs (Christensen, 1985). Seismic velocities were measured as a function of confining pressure, using the pulse transmission technique (Birch, 1960). This method measures the transmission time of a mechanical pulse along the length of the core, and then translates that time into a velocity. To generate the compressional wave pulse and the shear wave pulse, different transducer assemblages are required. Special care must be taken when obtaining shear wave velocities, to ensure that all possible combinations of propagation and vibration directions are measured. Shear wave velocities provide key information about crustal structure and composition, plus Poisson's ratios (e.g., McCormack et al., 1984; Holbrook et al., 1988; Ward and Warner, 1989; Johnston and Christensen, 1992; Christensen, 1996). Anisotropy is defined as the difference between the maximum and minimum velocities, expressed as a percentage of the mean velocity for each sample.

The velocity measurements were conducted at hydrostatic confining pressures up to 600 MPa to determine the influence of microcracks and mineralogy on the velocities. Fig. 3 shows a typical velocity versus pressure curve increasing rapidly below 100 MPa, due to crack closure (Birch, 1960, 1961), and increasing linearly above 100 MPa. Therefore, seismic properties will be examined at 150 MPa to enable a useful correlation with the LARSE data. The average, density, velocities, and anisotropy determined from the three minicores are listed in Table 3. Velocities are given at pressures of 150 MPa where the effects of cracks are largely eliminated. The LARSE velocity model loses resolution below 6 km depth (Lutter et

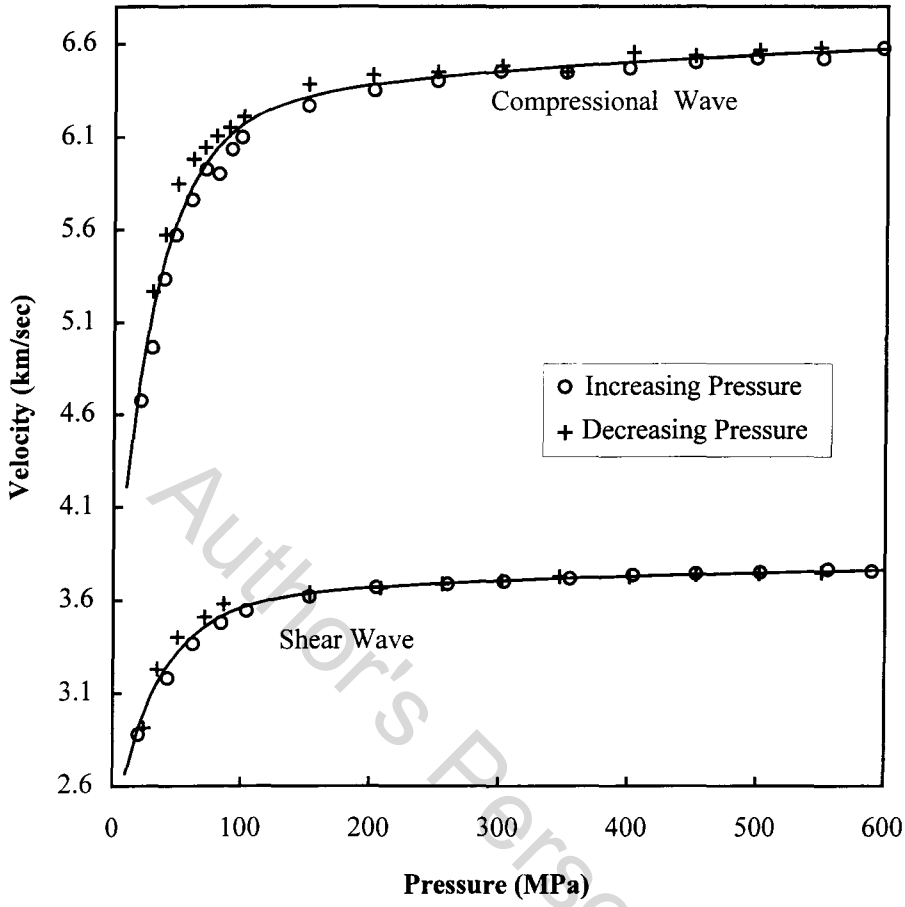

Fig. 3. Compressional and shear wave velocity presented as a function of pressure for NG-19A. Shear wave is propagating parallel to the lineation.

al., 1995), a confining pressure of approximately 170 MPa. A complete listing of the measured properties can be acquired from the authors upon request.

4. Seismic properties

Interpretation of seismic images using measured seismic properties requires understanding how composition and mineral fabrics produce variations in seismic velocity, anisotropy, and Poisson's ratio. Fig. 4 illustrates the commonly observed relationship of increasing velocity with increasing density (e.g., Birch, 1960; Christensen, 1965, 1966) associated with a progressive change in mineralogy from quartzo-feldspathic rocks to amphibole and pyroxene-rich rocks. In Fig. 4, average compressional and shear wave velocities at 150 MPa are plotted versus bulk densities at atmospheric pressure, as a function of lithology for each of the 39 samples. No one simple mathematical relationship can define the entire data set, because variations in mineralogy produce significant scatter in the data. For example the compressional velocities measured on the Pelona schist show a linear increase of velocity with density, whereas the Mojave gneisses have a wide range in velocity, but similar densities (Fig. 4a). Shear wave velocities appear more scattered due to a strong influence of quartz. Quartz has an extremely high shear wave velocity for its relatively low density (Christensen, 1966; Christensen and Fountain, 1975). Thus, samples rich in quartz, such as the Pelona schist, deviate substantially from the general

Table 3
Sample description and seismic properties

Sample	Description	Mineralogy	Ave. ρ (kg/m^3)	Pressure 150 MPa				
				Ave. V_p (km/s^2)	Ave. V_s (km/s^2)	% An. V_p	% An. V_s	Ave. σ
Southwest of San Andreas (San Gabriel)								
Gneisses:								
CP-3	Quartz feldspar gneiss	45% F; 35% Q; 10% E; 5% B	2673	5.749	3.541	3.4	9.2	0.194
CP-4	Quartz feldspar gneiss	40% Q; 30% F; 15% M; 10% E	2675	5.989	3.403	10.5	15.8	0.261
PB-6	Mafic gneiss	60% Ah; 30% F; 10% B	2972	6.137	3.6	11.5	15.5	0.238
NG-67	Quartz feldspar gneiss	45% F; 40% Q; 10% B	2655	5.908	3.494	2.0	0.6	0.231
NG-64	Quartz feldspar gneiss	50% F; 30% Q; 10% B; 5% Ch; 5% G	2769	5.983	3.665	3.4	0.2	0.2
NG-65	Mafic gneiss	40% Ah; 40% F; 15% B; 5% Ch	2936	6.299	3.62	2.0	6.9	0.253
NG-66	Mafic gneiss	40% Ah; 30% F; 15% B; 10% Q; 5% Ch	2843	6.03	3.604	3.0	2.0	0.222
Mendenhall gneiss:								
PC-24	Granulite quartz feldspar gneiss	45% F; 40% Q; 5% B; 5% Ah; 5% Ch	2694	6.01	3.552	2.1	2.5	0.232
PC-18	Granulite mafic gneiss	45% P; 40% F; 10% Ah	3064	6.907	3.856	0.3	2.3	0.274
Intrusives:								
PB-5	Biotite granite	45% F; 30% Q; 10% B; 5% E; 5% Ch	2631	5.639	3.319	1.1	0.7	0.235
J-24	Granite	70% F; 30% Q	2579	6.077	3.276	na	na	0.259
J-60	Diorite	50% F; 20% Ah; 15% Q; 15% B	2795	6.325	3.541	1.6	2.1	0.272
NG-39	Granite	60% F; 35% Q; 5% B	2571	5.747	3.664	2.0	7.4	0.158
NG-40	Biotite granite	60% F; 30% Q; 10% B	2616	5.811	3.241	4.2	2.8	0.274
NG-19	Granodiorite	55% F; 30% Q; 15% B	2688	6.224	3.623	3.0	0.4	0.243
Mt. Lowe intrusive:								
GR-24	Granodiorite	50% F; 35% Q; 10% E; 5% B	2655	6.069	3.534	0.1	4.6	0.243
GR-26	Granodiorite	60% F; 35% Q; 5% B	2621	5.816	3.329	2.4	0.1	0.256
Anorthosite complex:								
SG-AN	Anorthosite	90% F	2666	6.435	3.308	3.9	3.6	0.32
A102-9	Gabbro	50% Aa; 20% F; 20% B	3089	6.346	3.543	0.1	0.1	0.274
A102-10	Syenite	60% F; 20% Ah; 10% Q; 10% B	2755	6.162	3.455	3.4	0.9	0.271

Table 3 (continued)

Sample	Description	Mineralogy	Ave. ρ (kg/m^3)	Pressure 150 MPa				
				Ave. V_p (km/s^2)	Ave. V_s (km/s^2)	% An. V_p	% An. V_s	Ave. σ
Pelona schist:								
P-1	Quartz mica schist	60% Q; 20% F; 8% B; 7% M; 5% E	2672	5.854	3.624	6.6	13.5	0.189
P-2	Quartz mica schist	55% Q; 15% F; 10% B; 10% M; 5% E	2648	5.579	3.507	0.3	10.8	0.173
LA-1	Mica schist	45% F; 35% M; 10% Q; 10% E	2720	5.81	3.397	15.0	12.6	0.24
LA-2	Mica schist	45% F; 30% M; 20% Q; 5% E	2725	5.857	3.291	15.2	19.0	0.269
BP-5	Actinolite schist	55% Aa; 30% E; 10% F	2926	6.104	3.523	7.3	8.0	0.25
CP-1	Actinolite schist	45% Aa; 35% E; 10% F; 5% Q	2962	6.438	3.83	10.3	9.3	0.226
CP-2	Actinolite schist	35% Ah; 20% Aa; 20% E; 15% Ch; 10% F	3030	6.289	3.765	8.2	6.4	0.221
Northeast of San Andreas (Mojave)								
Gneiss:								
BP-1	Quartz feldspar gneiss	50% F; 35% B; 15% Q	2771	5.779	3.29	7.2	10.9	0.26
BP-4	Quartz feldspar gneiss	45% F; 20% Q; 20% Ah; 10% B; 5% Ch	2775	6.051	3.654	3.1	4.5	0.213
BP-7	Mafic gneiss	45% Ah; 35% F; 10% B; 5% Q; 5% E	2896	6.135	3.589	3.6	5.1	0.24
BP-2	Marble	90% C; 5% M	2787	6.639	3.693	10.4	9.8	0.276
BP-3	Marble	95% C	2656	6.434	3.401	1.5	1.4	0.306
Intrusives:								
P-13	Muscovite granite	65% F; 20% Q; 15% M	2557	5.714	3.459	3.3	0.9	0.211
BP-8	Granodiorite	65% F; 20% Q; 10% B	2527	5.467	3.218	5.7	5.4	0.235
SC-1	Granite	70% F; 25% Q; 5% B	2541	5.285	3.159	2.0	2.4	0.222
CP-7	Diorite	60% F; 10% B; 10% Ch; 5% Q; 5% Ah	2788	6.055	3.451	2.0	1.3	0.259
San Andreas fault zone								
P-6	**Felsic cataclasite**	**50% Q; 25% F; 20% C**	**2529**	**5.344**	**3.248**	**1.8**	**2.7**	**0.207**
PB-1	**Felsic cataclasite**	**60% Q; 35% F**	**2313**	**4.607**	**2.731**	**0.0**	**1.2**	**0.229**
PB-2	**Mafic cataclasite**	**45% Ah; 30% F; 10% B; 10% Ch; 5% Q**	**2604**	**5.049**	**2.917**	**2.7**	**3.0**	**0.25**

ρ = density; V_p = compressional waves; V_s = shear waves; An. = anisotropy; σ = Poisson's ratio; na = not available; Q = quartz; M = muscovite; B = biotite; F = feldspar (K-spar and plagioclase); Ah = hornblende; Aa = actinolite; P = pyroxene; G = garnet; Ch = chlorite; C = calcite; E = epidote.

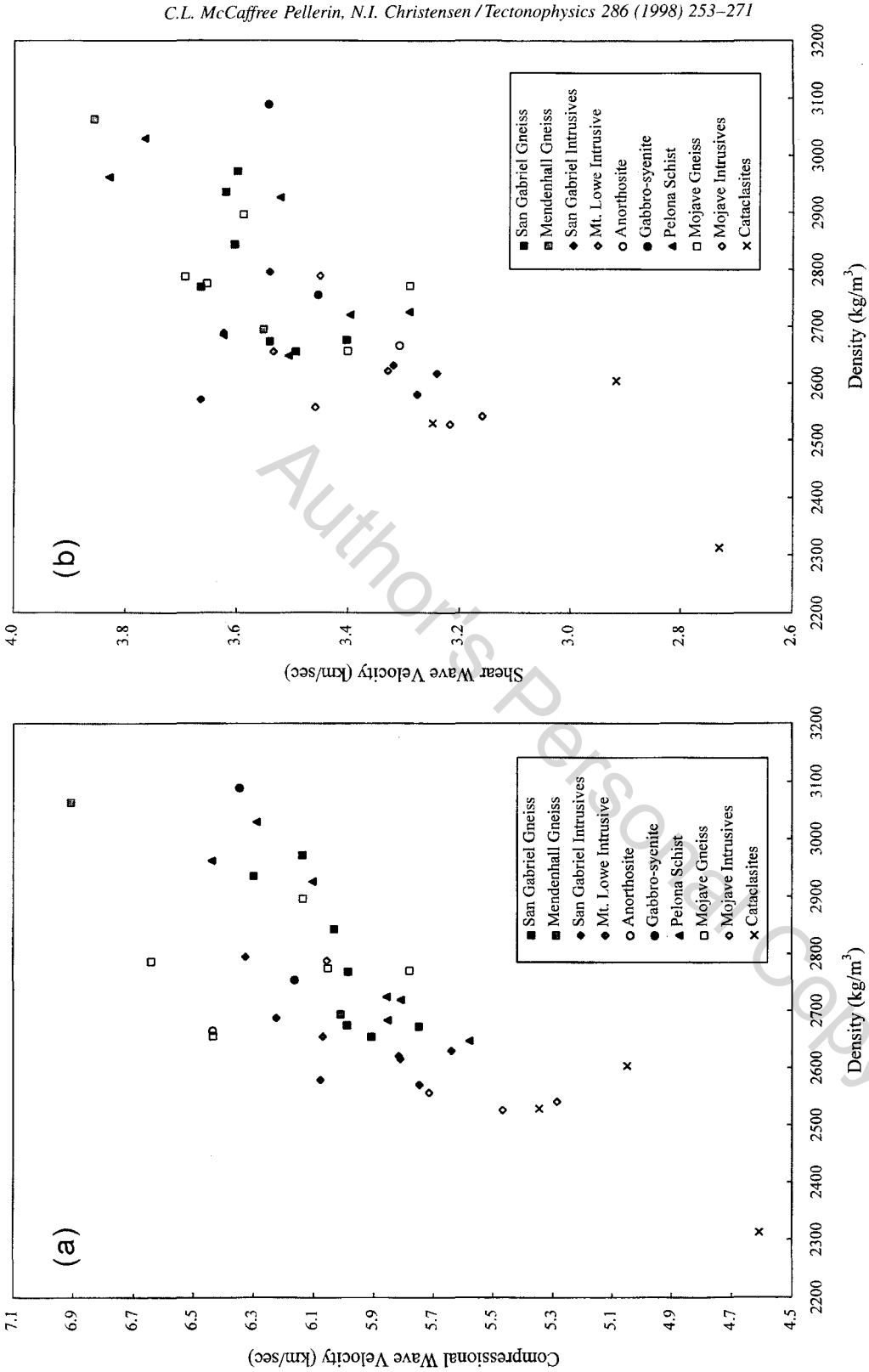

Fig. 4. (a) Average compressional velocities plotted versus density as a function of lithology. (b) Average shear wave velocities plotted versus density as a function of lithology.

trend of increasing shear wave velocity with increasing density (Fig. 4b).

Fig. 4 also illustrates how the wide range of velocities and densities relate to the lithologies in the SG-M region. The details of these relationships are summarized in Table 3. Average densities range from 2320 kg/m^3 for a fault zone cataclasite to 3100 kg/m^3 for a Mendenhall granulite gneiss. The fastest velocities are found in lithologies rich in feldspar, amphiboles, and pyroxenes, like the Mendenhall mafic granulite gneiss and amphibole schists. The anorthosite and marbles also have high velocities. The cataclasites exhibit the slowest velocities due to the intense deformation and alteration found in these samples. The quartzo-feldspathic samples represent the remaining velocities.

4.1. Anisotropy

Seismic anisotropy has become a significant tool for characterizing both rock types and crustal structures. Anisotropy influences seismic data by causing azimuthal variations in refraction profiles (e.g., Brocher and Christensen, 1990), increasing crustal reflectivity (Christensen and Szymanski, 1988; McCaffree and Christensen, 1993), and aligning split shear wave arrivals along dominant structural trends (Mjelde, 1991; Kern and Wenk, 1990; Zhang and Schwartz, 1994). Recent observations of crustal anisotropy in metamorphic terranes (Brocher and Christensen, 1990) and active fault zones (Zhang and Schwartz, 1994) suggest that anisotropy may be important in the interpretation of seismic data throughout the SG-M region.

In Fig. 5, compressional anisotropy is plotted versus shear wave anisotropy for the lithologies of the SG-M region. The gneisses and schists show significant compressional and shear wave anisotropy (5–20%), while most other rocks are nearly isotropic. Seismic anisotropy is generally attributed to either preferred mineral orientation (Christensen, 1965, 1966) and/or aligned fractures (Crampin, 1985).

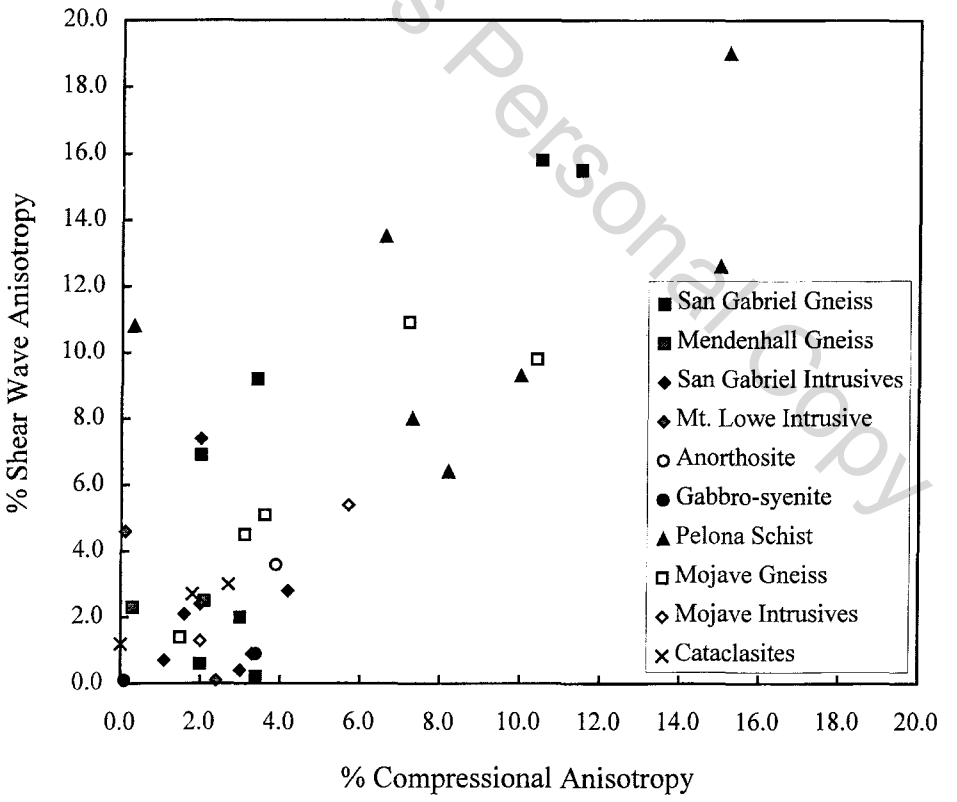

Fig. 5. Plot of shear wave anisotropy versus compressional anisotropy as a function of lithology.

Anisotropy due to microcracks and fractures is eliminated by using velocities at 150 MPa. Therefore, the observed anisotropy is produced by the preferred orientation of minerals such as the micas and amphiboles in the gneisses and schists. The orientation of the foliation exhibited by the gneisses and schists across the region will govern the degree to which anisotropy is detected on seismic data. The regional extent of the gneissic foliation has been destroyed by the intrusion of the Mesozoic rocks (Dibblee, 1982), minimizing the anisotropy. The Pelona schist, on the other hand, has a simple and pervasive foliation (Jacobson, 1983, 1988) that could produce significant velocity variation.

The Pelona schist anisotropy is discussed separately for each side of the San Andreas fault, since the orientation of the foliation differs in each terrane. In the Mojave terrane, seismic reflection data suggest that the Pelona schist foliation has a horizontal orientation (Cheadle et al., 1986). In the case of horizontal foliation, compressional waves propagating in the foliation plane travel at a high velocity with little azimuthal velocity variation, producing no observable anisotropy. In the San Gabriel terrane, the Pelona schist foliation ranges in dip from 45° to near vertical (Jacobson, 1983, 1988). Vertical foliation can produce a maximum compressional velocity variation for horizontal propagation of seismic waves with the fast velocity being recorded parallel to the foliation. The difference between the fast and slow compressional velocities defines the azimuthal anisotropy that would be recorded on refraction profiles. For the Pelona schist with vertical foliation, this azimuthal variation could be as much as 0.8 km/s.

Shear wave anisotropy in a vertically foliated section of Pelona schist causes a vertically propagating wave to split into two waves, with one traveling faster than the other. The difference in travel time between the split shear arrivals was calculated to be a maximum of 0.4 s for a 1 km-thick section of Pelona schist using the maximum shear wave velocity difference. Therefore, shear wave splitting measured in the vicinity of the San Andreas fault (Savage et al., 1990; Ozalaybey and Savage, 1995) can be explained by either mineral orientation in a section of Pelona schist along the fault or oriented fractures due to crustal stresses. These calculations of anisotropy support conclusions made by Brocher and Christensen (1990), who cautioned that erroneous interpretations can be made when interpreting crustal composition from a single azimuth refraction profile, or making inferences about principal stress directions in continental metamorphic terranes with significant anisotropy, like the SG-M region.

4.2. Poisson's ratio

Recent seismic field and laboratory studies have shown the usefulness of Poisson's ratios in determining crustal composition (Holbrook et al., 1988; Johnson and Hartman, 1991; White et al., 1992; Christensen, 1996). Average Poisson's ratios were calculated for each lithology in the SG-M region as a function of pressure (Fig. 6). The equation used to calculate the Poisson's ratio is:

$$\sigma = \frac{1}{2}\left[1 - \frac{1}{(V_p/V_s)^2 - 1}\right]$$

where V_p and V_s represent the weighted average compressional and shear wave velocity for each lithology. Table 4 lists the weighted lithologic average densities, velocities, and Poisson's ratios at 150 MPa. The weighting factors used to calculate the average velocities are the percent volume distributions estimated for each lithology (Table 2). In general, 10% errors in estimating the weighting factors produce errors of less than 0.05 km/s in the average velocities.

Fig. 6 shows that the SG-M region contains three distinct ranges of Poisson's ratios. The anorthosite complex exhibits the highest ratio (0.29), similar to anorthosites in other crustal studies (White et al., 1992; Christensen, 1996). This Poisson's ratio is less than that measured for pure anorthosite, 0.32, because the gabbroic and syenitic components were included in the average. The lowest Poisson's ratios that relate to high quartz content range from 0.22 for San Gabriel gneiss to 0.24 for the fault zone cataclasites. Previous studies have documented this relationship of decreasing Poisson's ratio with increasing quartz content (Christensen and Fountain, 1975; Wilkens et al., 1984; McCaffree and Christensen, 1993; Christensen, 1996). The remaining lithologies have average Poisson's ratios near 0.26, which is slightly lower than the average continental

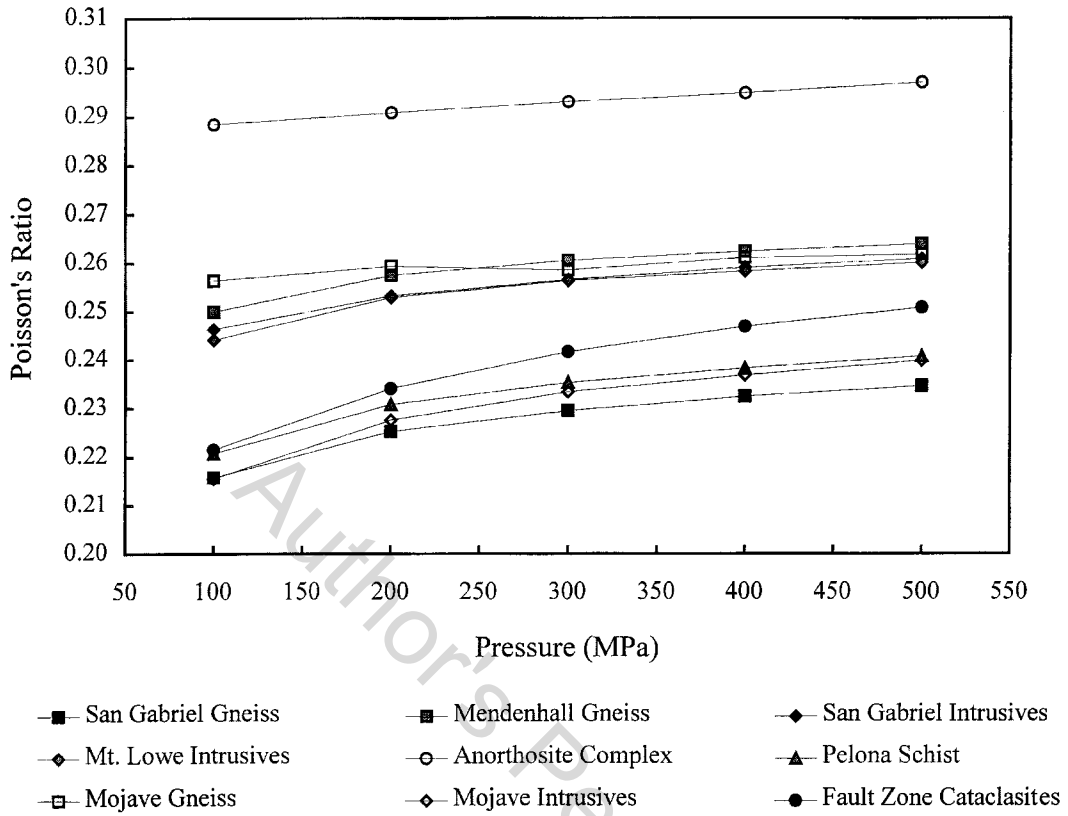

Fig. 6. Weighted lithologic Poisson's ratios plotted as a function of pressure.

crust ratio of 0.27 determined by Christensen (1996). The distinctive range in Poisson's ratio measured for the SG-M region suggests that field determination of Poisson's ratios may allow differentiation of major lithologies, such as the anorthosite, the Pelona schist, and the granulite gneisses.

Table 4
Lithologic weighted averages at 150 MPa (~5 km depth)

Lithologies	Density (kg/m^3)	V_p (km/s)	V_s (km/s)	Poisson's ratio (σ)
Southwest of San Andreas (San Gabriel)				
Gneiss	2805	6.031	3.567	0.231
Mendenhall gneiss	2879	6.459	3.704	0.255
Intrusives	2696	6.087	3.475	0.258
Mt. Lowe intrusive	2638	5.942	3.432	0.250
Anorthosite complex	2727	6.346	3.371	0.303
Pelona schist	2719	5.825	3.48	0.222
Northeast of San Andreas (Mojave)				
Gneiss	2830	6.045	3.531	0.241
Intrusives	2598	5.630	3.299	0.239
San Andreas fault zone				
Cataclasites	2482	5.000	2.965	0.229

V_p = compressional waves; V_s = shear waves.

5. Seismic interpretations

The following discussion includes a brief description of the seismic structure in the SG-M region and a comparison of the velocity structure with the laboratory velocities. The first refraction survey across the Transverse Ranges and Mojave Desert used travel time data from local seismic networks to obtain a one-dimensional crustal and upper mantle seismic velocity model. This velocity model shows 30 km of crust divided into three crustal layers having velocities of 5.5, 6.2, and 6.7 km/s with a mantle velocity of 7.8 km/s (Hadley and Kanamori, 1977). In this model, the upper crust with a velocity of less than 6.2 km/s exhibits a thickness variation across the San Andreas fault, with the Mojave region being thicker (~20 km) than the San Gabriel region (~10 km). Using airgun sources in the Bouquet reservoir, Malin et al. (1981) determined similar velocity models both parallel and perpendicular to the San Andreas fault, near Palmdale. Malin et al. (1981) also observed a thicker upper crust in the Mojave region. Hearn and Clayton (1986) established a similar change in crustal structure with a tomographic image, which shows a significant velocity variation across the San Andreas fault. The observed upper crustal velocities (5.5–6.2 km/s) correspond with the range of velocities measured at 150 MPa (~5 km depth) for crustal lithologies in the SG-M region (Table 4).

The LARSE experiment, using refraction and wide-angle reflection methods, has provided the most recent two-dimensional velocity model across the SG-M region (Fig. 7). The Line 1 survey consisted of 622 receivers spaced at 100-m intervals and 64 explosive sources at 1000-m intervals (Hafner and Clayton, 1995; Fuis et al., 1996). The velocity model was created by inversion of the first arrivals along Line 1, and has good resolution above 6 km depth (Lutter et al., 1995). The upper crustal velocities range from 4.5 to 6.5 km/s, similar to both the earlier one-dimensional velocity model and the laboratory velocities. The dominant features in the model are a dipping high-velocity zone, low-velocity sedimentary basins and low-velocity fault zones (Lutter et al., 1995; Fuis et al., 1996). The high-velocity anomaly dips to the southwest beneath the San Gabriel Mountains and exhibits a velocity increase on the order of 0.5 km/s. The sedimentary basins have a velocity range of 2.0–4.5 km/s and can be as deep as 2.5 km. Velocities associated with the San Andreas fault zone are 0.25 km/s lower than the adjacent crustal velocities. Except for the San Gabriel fault zone, similar velocity decreases are observed related to other faults in the region.

We will compare the LARSE velocity results with the laboratory velocities using two models, a constant-pressure model and a gradient model. The constant-pressure model examines the relationship between the lateral velocity anomalies described above and changes in rock composition. Such a comparison requires the LARSE velocities and the laboratory velocities to be at equivalent pressures. Thus depth in the LARSE model is converted to pressure using the relationship that hydrostatic confining pressure is proportional to the product of crustal density and the overlying rock thickness. This conversion assumed a constant crustal density of 2750 kg/m^3, to create the constant-pressure profile line at 150 MPa shown in Fig. 7. The constant-pressure line approximates topography because constant hydrostatic pressure and constant density imply uniform thickness of overlying rock.

Velocities, from the constant-pressure line of Fig. 7, are plotted as a solid bold line in Fig. 8. Weighted average laboratory velocities at 150 MPa for the major lithologies in the region are shown as constant-velocity lines. These weighted averages, which are given in Table 4, were calculated from the average sample velocities for each lithology and their estimated volume percentages from Table 2. The major fault zones are also marked on Fig. 8.

The following interpretation of crustal composition in the region is based on comparison of the weighted average laboratory velocities with the refraction velocities at depths corresponding to 150 MPa pressure (Fig. 8). This comparison is strictly valid for depths in the 3–6 km range (Fig. 7). The majority of lithologies found in the SG-M region exhibit typical crustal velocities (5.7–6.1 km/s), indicating that the upper crust consists of granitic intrusives and gneisses. Each terrane can be interpreted individually to provide a more detailed description of crustal composition. In the Mojave terrane, the Mojave gneiss represents the major lithology of the upper crust, with no evidence of any Pelona schist. This observation agrees with the Cajon drill hole results that also showed predominantly gneisses in the upper crust (Silver and James, 1988). The velocity

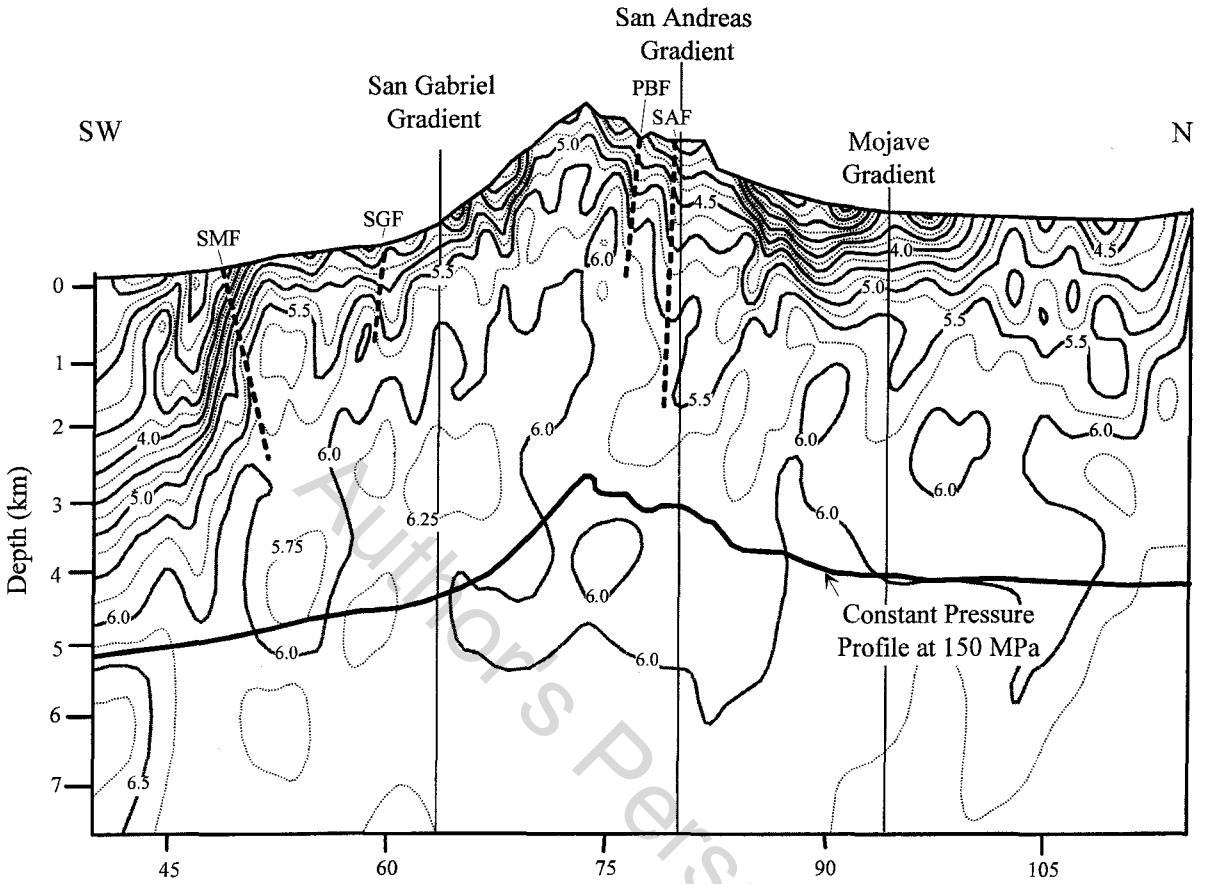

Fig. 7. LARSE Line 1 two-dimensional velocity model modified from Lutter et al. (1995). The constant-pressure profile line is marked with the bold line. The three gradient models are vertical lines labeled at the top. Contour interval is 0.25 km/s. Distance is measured from the first shot point to the southwest. *SGF* = San Gabriel fault; *SMF* = Sierra Madre fault; *SAF* = San Andreas fault; *PBF* = Punchbowl fault.

high on the northeast end is most likely a feature of poor resolution in the seismic data. Southwest of the San Andreas in the San Gabriel terrane there are three significant observations. First, fault zone cataclasites have much lower velocities than the velocity decrease associated with the San Andreas and Sierra Madre fault zones, implying that the narrow bands of cataclasite observed in the San Andreas have limited influence on the crustal velocities. The velocity decrease could also originate from a section of Pelona schist near the San Andreas fault. This interpretation is reasonable because the Pelona schist is exposed along the San Andreas fault in this region. Just west of the San Andreas velocity low, the crust has velocities similar to the San Gabriel gneiss, the San Gabriel intrusives, the Mt. Lowe intrusives and the Pelona schist. Lastly, the high-velocity anomaly near the San Gabriel fault correlates with anorthosite and/or crustal granulitic gneisses, suggesting either a massive anorthositic intrusion during the pre-Cambrian or a significant period of crustal uplift.

The gradient model determines how composition changes with depth by comparing crustal velocity gradients and velocity depth curves of the weighted lithologic averages (Fig. 9). Three different crustal gradients were chosen and marked on Fig. 7, to represent the velocity variations beneath each crustal regime: the San Gabriel Mountains, the San Andreas fault, and the Mojave Desert. In Fig. 9, the weighted average velocities and the velocity gradients are both

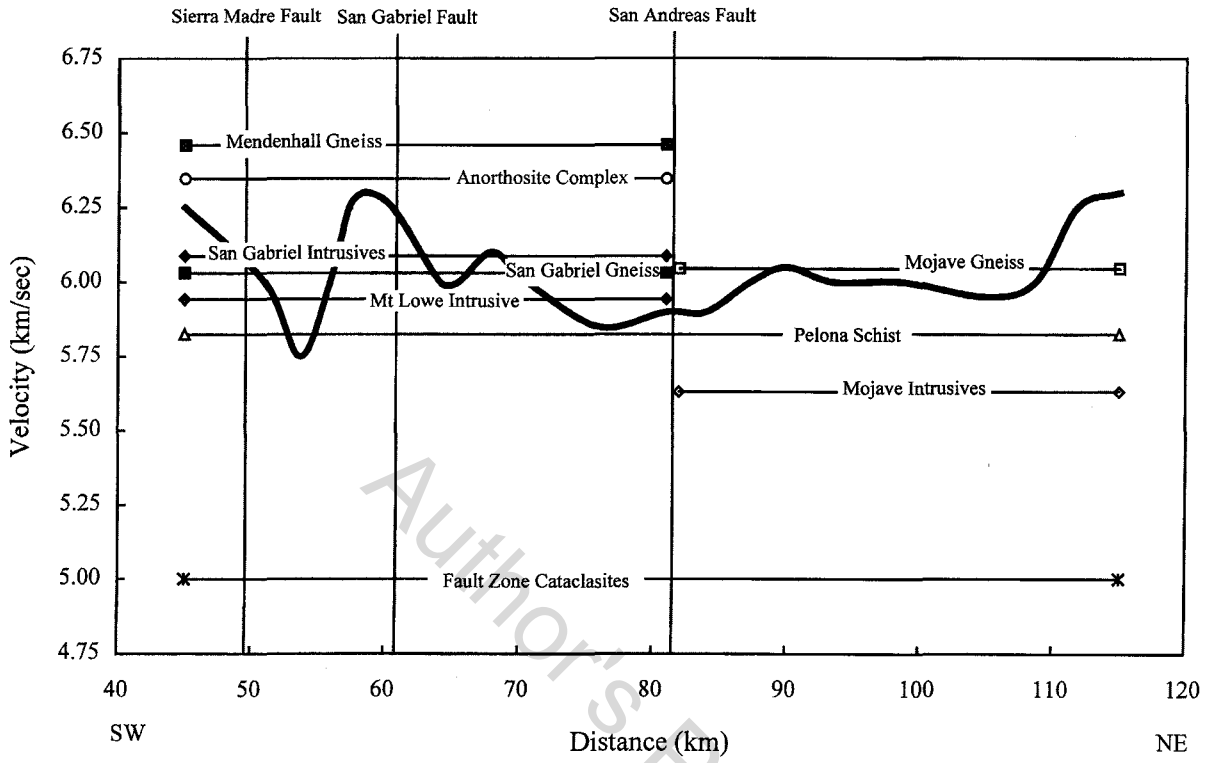

Fig. 8. Constant-pressure model presented at 150 MPa. LARSE velocity variations represented by the bold line. Weighted lithologic averages are plotted as constant-velocity lines.

plotted as a function of depth from the surface to maintain the pressure–depth relationship. None of the gradient profiles follow one single lithology with depth, indicating that the vertical variations in velocity are due to changes in lithology, not pressure. The gradients in the shallow crust (0–3 km) are hard to interpret due to unknown crustal fracturing. Interpretation of the upper crust (3–6 km) with the gradient model corroborates the findings of the constant-pressure model. The upper crust of the Mojave terrane contains mainly Mojave gneiss. As was previously discussed, the San Andreas fault zone velocity gradient agrees well with Pelona schist velocities. Finally, the velocity high under the San Gabriel terrane corresponds with the anorthosite and granulite gneisses.

6. Summary

The interpretation of rock composition beneath the SG-M region is still open to much debate. The laboratory velocities presented in this study show several important correlations with lithology. Compressional and shear wave velocities in the SG-M region increase with increasing density due to a progressive change in mineralogy from rocks with abundant quartz and feldspars to rocks containing amphiboles and pyroxenes. Compositional variations also produce a distinct range of densities and velocities associated with each lithology. Densities range from 2320 kg/m^3 for fault zone cataclasites to 3100 kg/m^3 for mafic granulite gneisses. Compressional wave velocities range from 4.61 km/s to 6.91 km/s and shear wave velocities range from 2.73 km/s to 3.86 km/s. Significant anisotropy (5–20%) is found in both gneisses and schists, and originates from preferred orientations of micas and amphiboles. Poisson's ratios range from 0.22 for the Pelona schist to 0.29 for the San Gabriel anorthosite. This wide range of Poisson's ratios allows lithologies, such as the anorthosite and the granulite gneiss, to be distinguished in the subsurface.

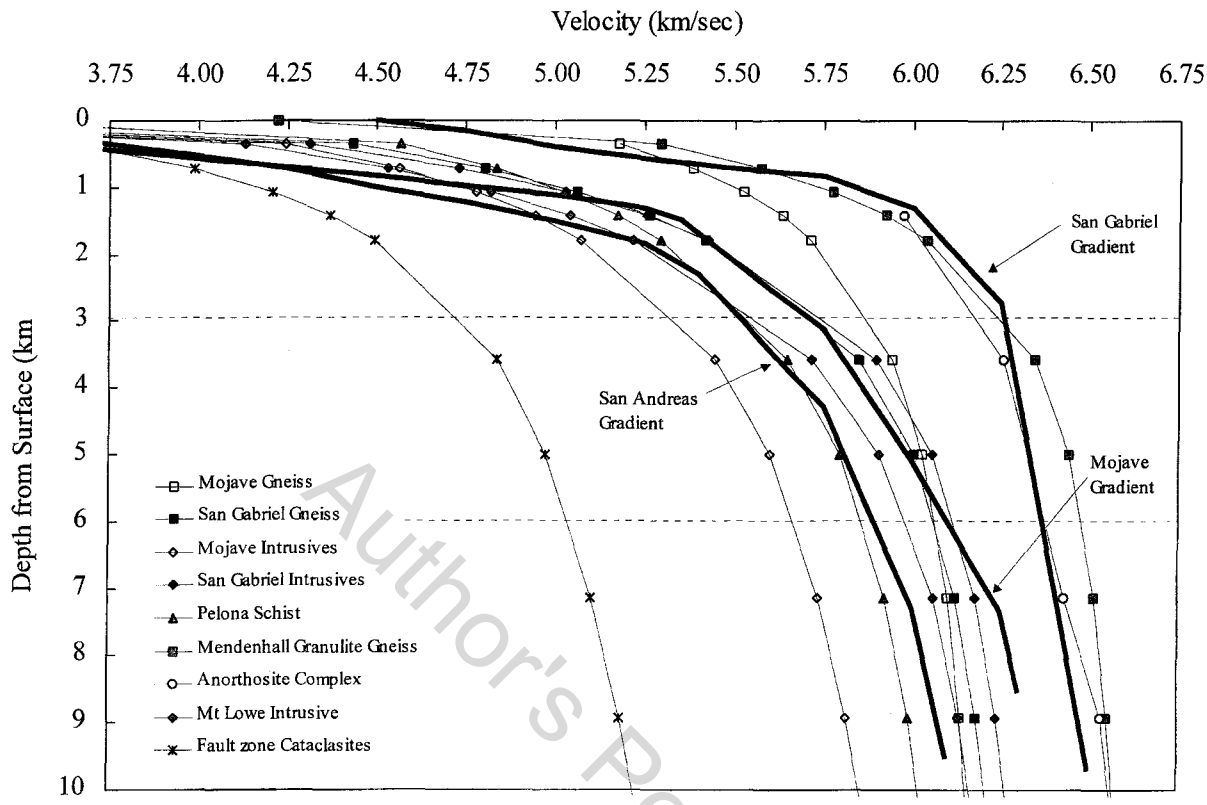

Fig. 9. Gradient model plotted as a function of velocity versus depth. Weighted lithologic velocities are marked by separate symbols. LARSE crustal gradients are plotted as bold lines and labeled. Dashed lines define the confidence interval of model.

Using laboratory velocities to interpret the LARSE data has resulted in constraints on crustal composition beneath the SG-M region. The upper crust in the Mojave terrane is primarily gneisses, while the San Gabriel upper crust consists of granitic intrusives, gneisses, and Pelona schist. Anorthosite and/or mafic granulite gneiss are correlated to the observed high-velocity anomaly on the LARSE model, suggesting either a period of anorthositic intrusion or eastward thrusting. Poisson's ratios can be used to differentiate these two interpretations, because anorthosite has a higher Poisson's ratio than granulite gneisses. The velocity decrease beneath the San Andreas fault zone could originate from minor amounts of cataclasite or the presence of low-velocity lithologies such as Pelona schist. This fault zone interpretation differs significantly from the central San Andreas fault zone model, supporting the conclusion of Mooney and Ginzburg (1986) that the southern San Andreas is governed by different fault mechanisms. This study could not interpret the lateral extent or subsurface geometry of the Pelona schist beneath the region, because the velocity of the schist falls within the crustal average. Observed reflectivity in crustal mylonites, high-grade metamorphic zones and the Rand schist (Cheadle et al., 1986; Matthews and Cheadle, 1986; Christensen and Szymanski, 1988; Wang et al., 1989; Li et al., 1992) suggest that the Pelona schist and/or the Vincent thrust may be highly reflective. If foliations are subhorizontal, this would provide a means to image the structure of the schist.

These results have contributed new information on crustal composition in the SG-M region, enhancing our understanding of the complex southern California geology. This new understanding of the subsurface geology will allow scientists to better assess earthquake hazards by depicting zones of future

seismic activity and providing additional parameters for modeling fault motions. For example, Magistrale and Zhou (1996) have shown that variations in crustal composition govern the maximum rupture depth for earthquakes. Further geophysical studies in this region, such as a 2-D Poisson's ratio model and reflectivity studies, will be important. The results of this study illustrate the utility of combining physical property measurements with field seismic studies to examine crustal structure, subsurface rock compositions, and fault zone properties.

Acknowledgements

We appreciate the assistance of G. Fuis and W. Lutter in providing us with the LARSE velocity model. We are grateful to D. Okaya, D. Szymanski, and S. McCaffree for field assistance. A. Barth generously provided several San Gabriel Mountain samples for velocity measurements. We also thank J. McBride and K. Favret for their constructive reviews. This work was supported by a Purdue David Ross Fellowship and the NSF Continental Dynamics Program, Grant EAR-9317522.

References

Anderson, J.L., Osborne, R.H., Palmer, D.F., 1980. Petrogenesis of cataclastic rocks within the San Andreas fault zone of southern California, U.S.A. Tectonophysics 67, 221–249.

Barth, A.P., 1990. Mid-crustal emplacement of Mesozoic plutons, San Gabriel Mountains, California, and implications for the geologic history of the San Gabriel terrane. Geol. Soc. Am. Mem. 174, 33–45.

Barth, A.P., Ehlig, P.L., 1988. Geochemistry and petrogenesis of the marginal zone of the Mount Lowe Intrusion, central San Gabriel Mountains, California. Contrib. Mineral. Petrol. 100, 192–204.

Birch, F., 1960. The velocity of compressional waves in rocks to 10 kilobars, 1. J. Geophys. Res. 65, 1083–1102.

Birch, F., 1961. The velocity of compressional waves in rocks to 10 kilobars, 2. J. Geophys. Res. 66, 2199–2224.

Brocher, T.M., Christensen, N.I., 1990. Seismic anisotropy due to preferred mineral orientation observed in shallow crustal rocks in southern Alaska. Geology 18, 737–740.

Burchfield, B.C., Davis, G.A., 1981. Mojave Desert and environs. In: Ernst, W.G. (Ed.), The Geotectonic Development of California. Prentice-Hall, Englewood Cliffs, N.J., pp. 216–252.

Carter, B.A., Silver, L.T., 1972. Structure and petrology of the San Gabriel anorthosite–syenite body, California. 24th International Geologic Congress, Montreal Rep., Section 2, pp. 303–311.

Cheadle, M.J., Czuchra, B.L., Byrne, T., Ando, C.J., Oliver, J.E., Brown, L.D., Malin, P.E., Phinney, R.A., 1986. The deep crustal structure of the Mojave Desert, California, from COCORP seismic reflection data. Tectonics 5, 293–320.

Christensen, N.I., 1965. Compressional wave velocities in metamorphic rocks at pressure to 10 kilobars. J. Geophys. Res. 70, 6148–6164.

Christensen, N.I., 1966. Shear wave velocities in metamorphic rocks at pressures to 10 kilobars. J. Geophys. Res. 71, 3549–3556.

Christensen, N.I., 1985. Measurements of dynamic properties of rock at elevated temperatures and pressures. In: Pincus, H.J., Hoskins, E.R. (Eds.), Measurements of Rock Properties at Elevated Pressures and Temperatures. American Society for Testing and Materials, Philadelphia, PA, ASTM STP 869, pp. 93–107.

Christensen, N.I., 1996. Poisson's ratio and crustal seismology. J. Geophys. Res. 101, 3139.

Christensen, N.I., Fountain, D.M., 1975. Constitution of the lower continental crust based on experimental studies of seismic velocities in granulites. Geol. Soc. Am. Bull. 86, 227–236.

Christensen, N.I., Szymanski, D.L., 1988. Origin of reflections from the Brevard Fault zone. J. Geophys. Res. 93, 1087–1102.

Crampin, S., 1985. Evaluation of anisotropy by shear-wave splitting. Geophysics 50, 142–152.

Crowell, J.C., 1981. An outline of the tectonic history of southeastern California. In: Ernst, W.G. (Ed.), The Geotectonic Development of California. Prentice-Hall, Englewood Cliffs, N.J., pp. 582–599.

Dibblee, T.W., Jr., 1975. Tectonics at the Western Mojave near the San Andreas Fault. Calif. Div. Mines Geol. Bull. 118, 155–161.

Dibblee, T.W., Jr., 1982. Geology of the San Gabriel Mountains, southern California. In: Fife, D.L., Minch, J.A. (Eds.), Geology and Mineral Wealth of the California Transverse Ranges. South Coast Geological Society Guidebook, No. 16, pp. 148–169.

Eberhart-Phillips, D., Micheal, A.J., 1994. Three-dimensional velocity structure, seismicity, and fault structure in the Parkfield region, central California. J. Geophys. Res. 98, 15737–15758.

Ehlig, P.L., 1975. Basement rocks on the San Gabriel Mountains, south of the San Andreas fault, Southern California. Calif. Div. Mines Geol. Bull. 118, 177–187.

Ehlig, P.L., 1981. Origin and tectonic history of the basement terrane of the San Gabriel Mountains, central Transverse Ranges. In: Ernst, W.G. (Ed.), The Geotectonic Development of California. Prentice-Hall, Englewood Cliffs, N.J., pp. 253–283.

Feng, R., McEvilly, T., 1983. Interpretation of seismic reflection profiling data for the structure of the San Andreas Fault Zone. Bull. Seismol. Soc. Am. 73 (6), 1701–1720.

Fuis, G., and 14 others, 1996. Images of crust beneath Southern California will aid study of earthquakes and their effects. EOS 77 (18), 173–176.

Hadley, D., Kanamori, H., 1977. Seismic structure of the Trans-

verse Ranges, California. Geol. Soc. Am. Bull. 88, 1469–1478.

Hafner, K., Clayton, R.W., 1995. Crustal structure beneath the San Gabriel Mountains, CA (LARSE). EOS 76 (46), F348.

Healy, J.H., Peake, L.G., 1975. Seismic velocity structure along a section of the San Andreas fault near Bear Valley, California. Seismol. Soc. Am. Bull. 65, 1177–1197.

Hearn, T.M., Clayton, R.W., 1986. Lateral velocity variations in southern California, I. Results for the upper crust from Pg waves. Seismol. Soc. Am. Bull. 76, 495–509.

Holbrook, W.S., Gajewski, P., Krammer, A., Prodehl, C., 1988. An interpretation of wide-angle compressional and shear wave data in southwest Germany: Poisson's ratio and petrological implications. J. Geophys. Res. 93, 12081–12106.

IUGS (International Union of Geological Sciences) Subcommission on the Systematics of Igneous Rocks, 1973. Plutonic rocks, classification and nomenclature. Geotimes 18, 26–30.

Jacobson, C.E., 1983. Structural geology of the Pelona Schist and Vincent thrust, San Gabriel Mountains, California. Geol. Soc. Am. Bull. 94, 753–767.

Jacobson, C.E., 1988. Structure, metamorphism, and tectonic significance of the Pelona, Orocpia, and Rand schists, southern California. In: Ernst, W.G. (Ed.), On Metamorphism and Crustal Evolution in Western U.S. Prentice-Hall, Englewood Cliffs, N.J., pp. 977–997.

Johnson, R.A., Hartman, K.A., 1991. Upper crustal Poisson's ratio in the Colorado Plateau from multicomponent wide-angle seismic recording. In: Meissner, R. et al. (Eds.), Continental Lithosphere: Deep Seismic Reflections. AGU, Geodyn. Ser. 22, 323–328.

Johnston, J.E., Christensen, N.I., 1992. Shear wave reflectivity, anisotropies, Poisson's ratios, and densities of a southern Appalachian Paleozoic sedimentary sequence. Tectonophysics 210, 1–20.

Kern, H., Wenk, H.-R., 1990. Fabric-related velocity anisotropy and shear wave splitting in rocks from the Santa Rosa Mylonite Zone. J. Geophys. Res. 95, 11213–11223.

Li, Y., Henyey, T.L., Silver, L.T., 1992. Aspects of the crustal structure of the Western Mojave Desert, California, from seismic reflection and gravity data. J. Geophys. Res. 97, 8805–8816.

Lutter, W.J., Thurber, C., Fuis, G.S., 1995. An image of the upper 5 km from inversion of first arrivals from the 1994 LARSE Experiment: Line 1 from Seal Beach to El Mirage Lake. EOS 76 (46), F348.

Magistrale, H., Zhou, H.-W., 1996. Lithologic control of the depth of earthquakes in southern California. Science 273, 639–643.

Malin, P.E., Gillespie, M.H., Leary, P.C., Henyey, T.L., 1981. Crustal structure near Palmdale, California, from borehole-determined ray parameters. Seismol. Soc. Am. Bull. 71, 1783–1803.

Matthews, D.H., Cheadle, M.J., 1986. Deep reflections from the Caledonides and comparison with the Himalayas. In: Barazang, M., Brown, L. (Eds.), Reflection Seismology: A Global Perspective. AGU, Geodyn. Ser. 13, 5–20.

May, D.J., 1989. Late Cretaceous intra-arc thrusting in southern California. Tectonics 8, 1159–1173.

McCaffree, C.L., Christensen, N.I., 1993. Shear wave properties and seismic imaging of mylonite zones. J. Geophys. Res. 98, 4423–4435.

McCormack, M.D., Dunbar, J.A., Sharp, W.W., 1984. A case study of stratigraphic interpretation using shear and compressional seismic data. Geophysics 49, 505–520.

Mjelde, R., 1991. Analysis of shear waves with respect to splitting near the San Andreas Fault. Int. J. Geophys. 107, 649.

Mooney, W.D., Ginzburg, A., 1986. Seismic measurements of the internal properties of fault zones. Pure Appl. Geophys. 124 (1/2), 141–157.

Ozalaybey, S., Savage, M.K., 1995. Shear-wave splitting beneath western United States in relation to plate tectonics. J. Geophys. Res. 100 (B9), 18135–18149.

Page, R.A., Boore, D.M., Bucknam, R.C., Thatcher, W.R., 1992. Goals, opportunities, and priorities for the USGS Earthquake Hazards Reduction Program. U.S. Geol. Surv., Circ. 1079.

Roller, J.C., Healy, J.H., 1963. Seismic refraction measurements of crustal structure between Santa Monica Bay and Lake Mead. J. Geophys. Res. 68, 5837–5850.

Savage, M.K., Silver, P.G., Meyer, R.P., 1990. Observations of teleseismic shear-wave splitting in the Basin and Range from portable and permanent stations. Geophys. Res. Lett. 17, 21–24.

Shedlock, K.M., Brocher, T.M., Harding, S.T., 1990. Shallow structure and deformation along the San Andreas fault in Cholame Valley, California, based on high-resolution reflection profiling. J. Geophys. Res. 95, 5003–5020.

Silver, L.T., James, E.W., 1988. Geologic setting and lithologic column of the Cajon Pass deep drillhole. Geophys. Res. Lett. 15, 941–944.

Stewart, R., Peselnick, L., 1978. Systematic behavior of compressional velocity in franciscan rocks at high pressure and temperature. J. Geophys. Res. 83, 831–839.

Wang, C., 1984. On the constitution of the San Andreas fault zone in central California. J. Geophys. Res. 89, 5858–5866.

Wang, C.Y., Okaya, D.A., Ruppert, C., Davis, G.A., Guo, T.S., Zhong, Z., Wenk, H.R., 1989. Seismic reflectivity of the Whipple Mountain shear zone in southern California. J. Geophys. Res. 94, 2989–3005.

Ward, G., Warner, M., 1989. Shear wave seismic reflections from the lower continental crust. EOS Trans. AGU 70 (43), 1203.

White, D.J., Milkereit, B., Salisbury, M.H., Percival, J.A., 1992. Crystalline lithology across the Kapuskasing uplift determined using in situ Poisson's ratio from seismic tomography. J. Geophys. Res. 97, 19993–20006.

Wilkens, R., Simmons, G., Caruso, L., 1984. The V_p/V_s as a discriminant of composition for siliceous limestones. Geophysics 49, 185–196.

Woodburne, M.O., 1975. Late Tertiary nonmarine rocks, Devil's Punchbowl and Cajon Valley, southern California. Calif. Div. Mines Geol. Bull. 118, 187–196.

Zhang, Z., Schwartz, S.Y., 1994. Seismic anisotropy in the shallow crust of the Loma Prieta segment of the San Andreas fault system. J. Geophys. Res. 99 (B5), 9651–9661.